Sec-O-glucosylhamaudol Inhibits RANKL-induced Osteoclastogenesis Via Repressing 5-LO and AKT/GSK3β Signaling

Jinjin Cao
Tongji University
Mingxue Zhou
Guangxi Traditional Chinese Medical University
Xinyan Chen
Tongji University
Menglu Sun
Tongji University
Congmin Wei
Tongji University
Qisheng Peng
Jilin University
Zhou Cheng
Tongji University
Wanchun sun (wanchunsun@jlu.edu.cn)
Jilin University https://orcid.org/0000-0003-0663-2255
Hongbing Wang
Tongji University

Research

Keywords: Sec-O-glucosylhamaudol, Osteoclast, NFATc1, GSK3β, 5-lipoxygenase, AKT

Posted Date: June 15th, 2021

DOI: https://doi.org/10.21203/rs.3.rs-582692/v1

Abstract

Background

Osteoclast excessive activation was closely related to bone diseases such as osteoporosis and rheumatoid arthritis. Sec-O-glucosylhamaudol (SOG), an active flavonoid compound derived from the root of divaricate *Saposhnikovia*, was reported to exhibit analgesic, anti-inflammatory and high 5-lipoxygenase (5-LO) inhibitory effects. However, its effect on osteoclastogenesis and bone resorption remained unclear.

Methods

Osteoclast formation, bone resorption pit area formation and F-actin ring formation were examined by TRAP staining, modified Vonkonsa staining and immunofluorescence, respectively. RT-Realtime PCR assay and western blot analysis were performed. siRNA transfection was conducted to silence the expression of 5-LO in cells. LPS-induced bone-loss mice model was prepared and the left and right femurs were collected for Micro-CT and histomorphometric analysis, respectively.

Results

SOG markedly attenuated RANKL-induced osteoclastogenesis through decreasing TRAP activity, F-actin ring formation and bone resorption with reduction of mRNA levels of osteoclastogenesis marker genes such as TRAP, CTSK and DC-STAMP. Our results further indicated that SOG markedly reduced the induction of key transcription factors NFATc1 and c-Fos at both mRNA and protein levels during osteoclastogenesis. In addition, SOG treatment did not alter the transient phosphorylation of NF-κB p65 subunit and MAPKs (p38, ERK1/2 and JNK), AKT and GSK3β by RANKL. Interestingly, our results showed that SOG significantly inhibited the phosphorylation of AKT and GSK3β at middle-late stage of osteoclastogenesis, but did not alter calcineurin catalytic subunit PP2B-Aα expression. GSK3β inhibitor SB415286 could partly reverse inhibition of osteoclastogenesis by SOG. 5-LO knockdown at BMMs also markedly reduced RANKL-induced osteoclastogenesis. In consistent with in vitro results，SOG could significantly improve bone destruction in LPS-induced mice model.

Conclusions

SOG attenuated formation and function of osteoclast through suppressing AKT-mediated GSK3β inactivation, and 5-LO catalytic activity. Moreover, SOG prevented LPS-induced bone loss in mice through inhibiting osteoclastogenesis. Taken together, this study provided the evidence that SOG may have a potential therapeutic effect on osteoclast-related bone lysis disease.

Background

Bone remodeling, a dynamic balance process, is regulated by bone formation of osteoblast and bone resorption of osteoclast[1]. Osteoclast hyperactivity mediated over resorption of bone tissue could lead to

bone loss, resulting in osteoporosis, rheumatoid arthritis, periodontitis, Paget's disease and bone tumor[2]. Previous studies suggested that inflammation and oxidative stress could promote osteoclast differentiation, leading to osteolysis[3,4]. Therefore, inhibition of excessive osteoclast formation and bone resorption activity has been regarded as an important therapeutic strategy for bone lysis diseases.

Macrophage-colony stimulating factor (M-CSF) and receptor activator of nuclear factor-κB ligand (RANKL) were regarded as master cytokines for osteoclast differentiation[5,6]. The binding of RANKL to RANK rapidly activate NF-κB, MAPK and c-Fos signaling[7,8]. These signaling pathways further cause initial induction of NFATc1, followed by auto-amplification of NFATc1. Coordinating with RANKL stimulation, immunoreceptor tyrosine-based activation motif (ITAM) signaling meditate Ca^{2+} oscillation and activation of calcineurin, followed by dephosphorylation of NFATc1 at its serine residues, leading to enhanced nuclear translocation of NFATc1[9]. Moreover, RANKL could induced inactivation of GSK3β, leading to termination of NFATc1 phosphorylation and promote osteoclastogenesis[10-12].

Sec-O-glucosylhamaudol (SOG) (Figure 1a) is an active flavonoid compound derived from the root of *Saposhnikovia* divaricate. In previous studies, SOG was found to have analgesic and anti-inflammatory activities[13-15]. In addition, SOG also exhibited high 5-lipoxygenase (5-LO) inhibitory effect[16]. However, the effect of SOG on RANKL-induced osteoclast differentiation and bone resorption remains unclear. In this study, we found SOG could strongly suppressed RANKL-induced osteoclast formation. We further investigated the molecular mechanism of SOG's inhibitory effects on osteoclastogenesis and examined the potential therapeutic effects of SOG using LPS-induced inflammatory bone lysis mice model.

Materials And Methods

Materials

Sec-O-glucosylhamaudol (Purity ≥ 95%) was provided by Nature Standard (Shanghai, China). Alpha modification of Eagle's minimum essential medium (α-MEM), fetal bovine serum (FBS), penicillin and streptomycin (PS) were purchased from Gibco (Grand Island, NY, USA). Recombinant murine M-CSF and RANKL were obtained from Prospec (Rehovot, Israel). SB415286 was purchased from Selleckchem (Houston, TX, USA). Lipopolysaccharide (LPS) from *Escherichia coli* O55:B5, 2,5-diphenyltetrazolium bromide (MTT), zoledronic acid (ZOL), tartrate-resistant acid phosphatase (TRAP) staining kit, rhodamine-phalloidin, 4',6-diamidine-2'-phenylindole dihydrochloride (DAPI), and all other chemicals were obtained from Sigma-Aldric (Saint Louis, MO, USA). Phospho-P65, NFATc1, c-Fos and PP2B-Aα were Santa Cruz Biotechnology (CA, USA). All other antibodies used in this study were obtained from Cell Signaling Technology (Danvers, MA, USA).

Cell culture and osteoclast differentiation

Murine bone marrow cells were separated from femur and tibia of 6-8 week-old mice and cultured in α-MEM supplemented with 10% FBS, 1% PS, and 30 ng/mL M-CSF for 24 h. The cell suspensions were seed

in 10 cm dish at 37 °C with 5% CO_2 for 2 d. The adherent cells were then reserved as BMMs.

For osteoclast differentiation, BMMs (7×10^4 cells/well) were seeded into 48-well plates and cultured with α-MEM complete medium supplemented with 30 ng/mL M-CSF and 100 ng/mL RANKL for 4 d. Various concentrations of SOG were added to cultures at indicated time. TRAP staining assay was performed as described previously[40]. TRAP-positive cells containing three or more than 3 nuclei were regarded as osteoclasts.

Cytotoxicity assay

BMMs (1.5×10^4 cells/well) were seeded into a 96-well plate and cultured with α-MEM complete medium containing 30 ng/mL M-CSF, 100 ng/mL RANKL and SOG (0-200 μM) for 24 h and 48 h respectively. After removing medium, 100 μL of MTT (0.5 mg/mL) solution was added to each well. After 4 h, the supernatant was discarded and 150 μL DMSO was added for dissolving formazan. The optical density (OD) were measured at 570 nm using a microplate reader.

F-actin ring formation assay

BMMs were seeded in 48-well plate at 7×10^4 cells per well and cultured with α-MEM complete medium containing 30 ng/mL M-CSF, 100 ng/mL RANKL and SOG (0-200 μM) for 4 d. Then cells were fixed with 4% Paraformaldehyde (PFA) for 20 min, then cells were permeabilized with 0.5% Triton X-100 for 5 min. After washing three times with PBS, phalloidin was used to stain F-actin for 30 min and DAPI was used to stain nuclei for 5 min. Fluorescence images were acquired on a fluorescence microscope (RVL-110-G, ECHO Labpratories).

Quantitative realtime-PCR assay

BMMs were seeded at 1×10^6 cells/well in a 6-well plate and cultured with α-MEM complete medium containing 30 ng/mL M-CSF, 100 ng/mL RANKL and SOG for the indicated periods. Total RNA was extracted using RNA EASY MINI KIT (Qiagen, Hilden, Germany) according to the manufacturer's instruction. Transcriptor First Strand cDNA Synthesis Kit (Roche, Mannheim, Germany) was used for reverse transcription of cDNA. The mRNA levels of osteoclast-related genes were evaluated by real-time PCR using a SYBR Green kit (Roche, Mannheim, Germany). GAPDH was served as an inner control gene. The primer sequences for the genes were shown in table1.

Table 1. Primers used for quantitative PCR

Primer sequence **5'-3'**

Gene	Forward	Reverse
TRAP	CACTCCCACCCTGAGATTTGT	CATCGTCTGCACGGTTCTG
CTSK	AATACCTCCCTCTCGATCCTACA	TGGTTCTTGACTGGAGTAACGTA
DC-STAMP	TACGTGGAGAGAAGCAAGGAA	ACACTGAGACGTGGTTTAGGAAT
c-Fos	CGGGTTTCAACGCCGACTA	TTGGCACTAGAGACGGACAGA
NFATc1	GGAGAGTCCGAGAATCGAGAT	GGAGAGTCCGAGAATCGAGAT
GAPDH	AGGTCGGTGTGAACGGATTTG	TGTAGACCATGTAGTTGAGGTCA

Bone resorption assay

BMMs were plated on a corning osteo assay surface 24 wells plate at a density of 1×10^5 cell/well and cultured with α-MEM complete medium containing 30 ng/mL M-CSF, 100 ng/mL RANKL and SOG (0-200 μM) for 4 d. At the end of culture period, the cells were removed with 5% sodium hypochlorite. Von Kossa staining was performed as previously described[41]. The resorption area was observed under a light microscope and analyzed using imageJ software. The results were expressed as a percentage of the total well area.

siRNA transfection of cells

BMMs were plated and cultured on 48 wells or 6 wells plate at 37 °C for 24 h. Next, BMMs were transfected with control siRNA or 5-LO siRNA at a final concentration of 50 nM using Ribo FECTTM CP Reagent (RiboBio, Guangzhou, China) according to the manufacturer's protocol. Control siRNA was used as negative control for possible nonspecific effects of RNA interference. Cells were harvested for western blot analysis.

Western blot assays

Cells were lysed using RIPA lysis buffer on ice and lysates were collected by centrifugation at 4 °C at 12000 rpm for 10 min. The equal amount of protein sample (30-50 μg) was separated by 10-12% SDS-page and transferred to a PVDF membrane. The membrane was blocked with 5% fat-free milk for 2 h and incubated with primary antibodies overnight at 4 °C. After washing 3 times with TBST, the membrane was incubated with HRP-conjugated second antibody for 2 h at room temperature. After washing 5 times with TBST, the protein bands were detected using enhanced chemiluminescence (ECL), the images were quantified by imageJ.

LPS-induced bone loss model

Female C57BL/6 mice (6 weeks old) were obtained from shanghai SLAC laboratory animal Co.ltd. The mice were housed in controlled environments of temperature (22 ± 2 °C) and humidity (53 ± 5 °C) under a 12 h light/dark cycle. Animal experiments were performed strictly according to the Guide for the Humane

Use and Care of Laboratory Animals (Animal protocol number: TJCAC-018-036). LPS-induced model of bone loss was performed as previously described[42,43]. The mice were randomly assigned to five groups (n=10): PBS control (Sham), LPS injection (LPS group; 5 mg/kg body weight), SOG injection (only SOG group), LPS in combination with 5 mg/kg body weight dose of zoledronic acid (ZOL group); LPS in combination with 10 mg/kg body weight dose of SOG (SOG group). SOG, ZOL, and LPS were injected intraperitoneally every other day for 8 d. Two hours after SOG or ZOL injection, LPS or PBS was then injected intraperitoneally. Mice were euthanized at 8th day after the first injection of LPS. The left and right femurs were collected for Micro-CT and histomorphometric analysis, respectively.

Micro-CT and histomorphometric analysis

The collected left femurs were fixed with 4% PFA for 24 h, and scanned by Micro-CT (Quantuun GX MicroCT system; PerkinElmer, Waltam Mass, USA). Bone mineral density (BMD), trabecular thickness (Tb.Th), trabecular number (Tb.N) and trabecular separation (Tb.Sp) were measured.

Right femur samples were demineralized in 10% EDTA for 2 weeks. The femur samples were embedded with paraffin and sectioned to 5 μm thickness and stained by hematoxylin and eosin (H&E), and tartrate-resistant acid phosphatase (TRAP) staining. A high-quality microscope was used to photograph slices.

Statistical analysis

GraphPad Prism7 (SanDiego, CA, USA) were used for data analysis. Data were expressed as mean ± SD. Differences between groups were examined using one-way Anova followed by the Student-Newman-Keul's test. $p < 0.05$ was considered significant.

Results

SOG inhibited RANKL-induced osteoclast formation

To evaluate the effect of SOG on RANKL-mediated differentiation, cells were cultured with treatment of M-CSF, RANKL, and indicated concentrations of SOG. Firstly, the potential cytotoxicity of SOG was evaluated. MTT assay showed that up to 200 μM of concentration, SOG did not exhibit obvious cytotoxic effects compared to cells without SOG treatment (Figure 1b). Further, the effects of SOG on osteoclast formation were determined. As shown in figure 1c, the number and size of osteoclasts were significantly inhibited by SOG treatment in a concentration-dependent manner.

Osteoclast differentiation goes through several stages including early, middle and late stage. To determine at which stage SOG could affect osteoclast formation, 200 μM SOG was added to BMMs at different stage of osteoclastogenesis (Figure 1e) and treatment lasted for 24 h. As figure 1d shown, SOG treatment alleviated the number and size of osteoclast at all stages of cell differentiation. However, SOG stronger inhibited osteoclast formation at middle and late stage (day 3 and day 4) compared to early

stage (day1 and day2) (Figure 1d). Taking together, these results suggested that SOG suppressed RANKL-induced osteoclastogenesis, especially at middle-late stage of cell differentiation.

SOG impairs osteoclastic resorption and F-actin ring formation.

Next, the effects of SOG treatment on osteoclast-mediated bone resorption and F-actin ring formation of osteoclasts were examined. It is acknowledged that the formation of well-defined F-actin ring was indispensable for osteoclastic function[4]. Figure 2a showed that the number and size of F-actin rings were effectively diminished with the increase of the concentration of SOG. Treatment with SOG also dose-dependently decrease the formation of bone resorption pits, in terms of pits area (Figure 2b). SOG treatment almost abolished resorption pits formation at the concentration of 200 μM. To investigate at which stage SOG exerted its inhibitory effects on bone resorption function of osteoclasts, 200 μM SOG was added to BMMs at day 1, 2, 3 and 4 during osteoclastogenesis for 24 h. Consistent with results shown at figure 1d, SOG exhibited stronger inhibition on bone resorption pits formation at middle-late stage (day 3 and day 4 after RANKL treatment) compared to that at early stage (Figure 2c). Collectively, these results indicated that SOG remarkably suppressed bone resorption function of osteoclasts, especially at middle-late stage of cell differentiation.

SOG repressed the induction of osteoclast specific genes

RANKL stimulation up-regulates osteoclast-related genes, which regulats the differentiation, maturation, and function of osteoclasts. NFATc1, a master transcription factors for osteoclastogenesis, regulats the expression of osteoclast specific genes[17]. To investigate the impacts of SOG on osteoclast-related genes, we used RT-PCR to examine the mRNA expression of these genes, including NFATc1, c-Fos, CTSK, TRAP, DC-STAMP. As figure 3a shown, mRNA expression of these genes was obviously enhanced by RANKL stimulation. Meanwhile, SOG treatment strongly suppressed mRNA level of these genes (Figure 3a and 3b). The expression of key transcription factors c-Fos and NFATc1 was significantly suppressed at both mRNA and protein levels with SOG treatment (Figure 3c).

In addition, to investigate the impacts of SOG on osteoclast-related genes at different stage of cell differentiation, BMMs were treated with SOG on day 1, 2, 3, 4 of osteoclastogenesis. We found that mRNA levels of target genes (TRAP, CTSK, DC-STAMP) were decreased with SOG at all stages of osteoclastogenesis (Figure 3d). However, mRNA levels of CTSK, TRAP and DC-STAMP were more remarkably suppressed at middle-late stage (Figure 3d). Meanwhile, the protein and mRNA levels of c-Fos and NFATc1 were suppressed by SOG at all stages of cell differentiation, but SOG existed stronger inhibition on protein and mRNA levels of c-Fos and NFATc1 at middle-late stage (day 3 and day 4 after RANKL treatment)(Figure 3e and 3f). These results suggested that SOG inhibited osteoclastogenesis by suppressing expression of c-Fos/NFATc1-mediated osteoclast specific genes.

The effect of SOG on NF-κB, MAPK and AKT-GSK3β pathways at initial stage of osteoclastogenesis

It has been reported that NF-κB, MAPK and AKT-GSK3β pathways play a vital role in early induction of NFATc1[18,19]. To further explore the molecular mechanism of SOG modulating NFATc1 signaling, the effects of SOG on RANKL-initiated transient activation of NF-κB, MAPK and AKT as well inactivation of GSK3β were evaluated by western blot assay. As figure 4a shown, RANKL-stimulation induced transient phosphorylation of NF-κB and MAPKs including p38, ERK1/2 and JNK, which was not altered with SOG treatment. As well, RANKL-induced transient activation AKT and subsequent GSK3β inactivation also were not affected with SOG treatment (Figure 4b). These results suggested that SOG treatment might not influence the initial induction of NFATc1 via modulation of NF-κB, MAPK and AKT-GSK3β signaling.

The effects of SOG on the RANKL-induced calcineurin /NFATc1 and AKT-GSK3β/NFATc1 signaling pathway during osteoclastogenesis

Activation of NFATc1 was regulated by calcineurin via dephosphorylation of NFATc1 at middle stage of osteoclastogenesis[20]. To investigate whether SOG could affect RANKL-induced middle-late signaling pathways, RANKL-stimulated BMMs were treated with SOG for 24 h at different periods of osteoclastogenesis, respectively. We found that the expression of calcineurin catalytic subunit PP2B-Aα was not obvious changed with treatment of SOG (Figure 5a, 5b).

GSK3β was negative regulator of NFATc1 through phosphorylation of serine residues of NFATc1[21]. AKT mediates inactivation of GSK3β via phosphorylating serine 9 residue of GSK3β which was required for osteoclastogenesis. As figure 5a shown, the relative levels of phosphorylation of AKT and GSK3β were alleviated with SOG treatment during middle-late stages of osteoclast differentiation. These results suggested that SOG might suppress NFATc1 activation via inhibition of AKT-mediated GSK3β inactivation.

Further, SB415286, a selective GSK3β inhibitor, was used to confirm whether SOG could suppress RANKL-induced osteoclast differentiation through inhibition of AKT-mediated GSK3β inactivation. As shown in figure 5b, addition of SB415286 partly weakened the inhibitory effect of SOG on osteoclasts formation at middle-late stage of cell differentiation.

Taken together, these data suggested that SOG repressed RANKL-induced osteoclast differentiation partly by inhibition of AKT-mediated GSK3β inactivation at middle-late stage of osteoclastogenesis.

The effects of Knockdown of 5-LO on RANKL-induced osteoclastogenesis

Previous study showed that SOG inhibited 5-lipoxygenase (5-LO) catalytic activity with an IC_{50} value of 7.45 μM in vitro[16]. In order to explore the potential role of 5-LO in suppression of SOG on osteoclast differentiation, the expression of 5-LO in BMMs was knock-down by siRNA. As figure 6a shown, 5-LO silencing by siRNA obviously inhibited osteoclast formation compared to siRNA control. In addition, RANKL-induced NFATc1 expression level were significantly attenuated in 5-LO siRNA transfected BMMs compared to siRNA control (Figure 6b). However, knockdown of 5-LO did not change phosphorylation levels of AKT and GSK3β (Figure 6b). Taken together, these data indicated that 5-LO knockdown

remarkably suppressed RANKL-induced osteoclastogenesis, but not through the AKT/GSK3β signaling pathway. SOG might also inhibit osteoclastogenesis through inhibition of 5-LO catalytic activity.

SOG treatment improved LPS-induced bone loss

Given that the inhibitory effects of SOG on osteoclastogenesis in vitro, we further evaluated the potential therapeutic effects of SOG on LPS-induced bone loss in mice model. 2D and 3D reconstruction images of Micro-CT revealed that LPS group developed a significant osteoporosis in femur compared with sham group (Figure 7a). And, ZOL group, as positive group, markedly reduced LPS-induced bone loss. Similarly, SOG treatment also significantly improved bone destruction in LPS-treated mice. Moreover, Alone SOG group had no obvious change in bone mass compared to sham group. Quantitative analysis of bone microparameters showed that SOG group increased the values of BMD, BV/TV and Tb.N and decreased in Tb.Sp value compared with LPS-treated group (Figure 7b). H&E staining further confirmed that SOG treatment significantly reduced LPS-induced bone destruction in mice model (Figure 7c). In addition, bone histomorphometric analyses with TRAP staining revealed that SOG group decreased the number of TRAP-positive osteoclasts compared with LPS group (Figure 7c). These observations indicated that SOG attenuated LPS-induced bone loss in mice.

Discussion

In this study, we demonstrated for the first time that SOG could significantly suppress RANKL-induced osteoclastogenesis. Meanwhile, in vivo experiment further indicated that SOG markedly improved LPS-induced bone loss in mice. Therefore, SOG might be a new treatment option for osteoclast-related bone lysis diseases. It is well-known that osteoclastogenesis is a complicated and multiple stage process. In present study, the effects of SOG on osteoclast differentiation at different stages of cell differentiation were explored. We found that SOG exhibited inhibitory effects during all periods of osteoclastogenesis, but SOG exhibited stronger inhibitory effect on osteoclast formation in the middle-late stage than early stage of cell differentiation.

It is generally accepted that NFATc1 plays a master role in RANKL-induced osteoclastogenesis and induction of osteoclast-specific genes[22]. These genes (such as TRAP, CTSK, DC-STAMP et al.) are regulated by NFATc1 via binding to the gene promoter region. CTSK could dissolve the mineralized and organic structures of bone[23,24]. DC-STAMP takes part in osteoclast fusion and formation[25,26]. In this study, we observed that SOG significantly suppressed RANKL-induced expression of NFATc1 and c-Fos at both mRNA and protein levels. Meanwhile, mRNA expression of TRAP, CTSK, DC-STAMP were obviously inhibited with treatment of SOG. These evidences showed that SOG suppressed osteoclastogenesis via reducing expression of TRAP, CTSK, and DC-STAMP by inhibition of NFATc1 and c-Fos.

Investigating the impacts of SOG in different stage of cell differentiation, we found that SOG down-regulated the expression of NFATc1, c-Fos and osteoclast-specific genes at each stage of cell differentiation. Interesting, in the middle and late stage of osteoclast differentiation, SOG showed

stronger inhibition. These suggested that SOG had stronger suppressive effects in the middle and late stage of osteoclastogenesis.

RANKL interacting with its receptor RANK initially activates early signaling pathways, such as NF-κB, MAPK and AKT-GSK3β signaling[18,27-30]. Meanwhile, these early signaling pathways induced the initial expression of NFATc1. However, SOG had no conspicuous inhibitory effects on phosphorylation of NF-κB p65 subunit, MAPKs (p38, JNK, and ERK1/2), AKT and GSK3β in response to RANKL transient stimulation. These findings implicated that SOG might not influence the initial induction of NFATc1 through modulation of early signaling pathways at the initial stage of cell differentiation.

Inducing activation of NFATc1 is continuous process. Calcineurin dephosphorylated NFATc1 at its serine residues. Following by, NFATc1 translocated into the nucleus and induced the expression of target genes. FK506, a calcineurin inhibitor, inhibited RANKL-induced osteoclastogenesis, even when it was added at late phase of osteoclastogenesis[22]. However, SOG did not alter expression of calcineurin catalytic subunit PP2B-Aα, implicated that SOG might not affect NFATc1 dephosphorylation via inhibition of calcineurin.

GSK3β-mediated phosphorylation of NFATc1 at serine residues promotes NFATc1 nuclear export and localization in the cytoplasm[21,31]. RANKL stimulates phosphorylation of GSK3β at serine 9 and inactivates GSK3β. GSK3β inactivation leads to promotion of nuclear localization of NFATc1 and osteoclastogenesis. GSK3β Ser-9 phosphorylation is a continuous process and increases to peak on day 3 after RANKL stimulation[32]. Accordingly, in this study, the phosphorylation of GSK3β reached its peak on 3 day of RANKL stimulation. Studies reported that ectopic expression of a constitutive active form of GSK-3β attenuated osteoclast formation through downregulation of NFATc1[10]. Consitently, our results showed that RANKL-induced GSK3β inactivation was markedly reduced with treatment of SOG on different period of osteoclastogenesis. Even adding SOG at the middle-late phase of osteoclastogenesis (day 3 and day 4 after RANKL stimulation), GSK3β phosphorylation was still remarkably suppressed. These results suggested that SOG might promoted NFATc1 phosphorylation through enhancement of GSK3β activation.

GSK3β inhibitors, kenpaullone, SB216763 and SB415286 promoted RANKL-induced osteoclastogenesis[32]. In this study, our results showed addition of 10 μM SB415286 partly weakened the inhibitory effect of SOG on osteoclasts formation at middle-late stage of cell differentiation, suggested that SOG inhibited osteoclast formation at least partly via reduction of GSK3β Ser-9 phosphorylation.

Previous studies confirmed the crucial role of AKT/GSK3β signaling in osteoclastogenesis[10]. RANKL-activated AKT could enhance GSK3β phosphorylation at ser-9 and inactivation, which lead to an enhanced accumulation of NFATc1 in the nucleus and promote osteoclastogenesis[33]. Ectopic expression of constitutive activated AKT increases the levels of inactive GSK3β and thereby enhances nuclear localization of NFATc1[10]. Hence, our data reveal that SOG strongly inhibited RANKL-induced AKT phosphorylation in middle-late stage (day 2-day 4) of osteoclastogenesis. Taken together, these results

suggested that SOG suppressed osteoclast formation partly by inhibiting AKT/GSK3β/NFATc1 signaling pathway.

Leukotrienes, inflammatory mediators, play an important role in development of inflammation. Several studies reported that leukotriene B4 (LTB4) via G protein coupled receptors BLT1 and BLT2 and cysteinyl leukotrienes via G protein-coupled receptors CysLT receptors promoted osteoclastogenesis[34-37]. 5-lipoxygenase (5-LO) is one of the key enzymes of the arachidonic acid cascade catalyzing the formation of bioactive leukotrienes. 5-LO plays an important role in inflammatory disorders and bone metabolism[38]. Lee et al. reported that silence of 5-LO expression diminished RANKL-induced osteoclastogenesis and the inhibitory effects of 5-LO knocking down on osteoclastogenesis might be contributed to blockage of autocrine of leukotrienes[37]. Another study indicated that K7, 5-LO inhibitor, markedly suppressed osteoclastogenesis via reducing NFATc1 expression[39]. A previous study reported that SOG exhibited inhibitory potency on 5-LO catalytic activity with an IC_{50} value of 7.45 μM in vitro[16]. Consistently, we found that SOG could effectively suppressed RANKL-induced osteoclast formation at a concentration range from 50 to 200 μM. Given the efficacy of SOG penetrating through cell membrane, this concentration range of SOG is similar with its IC50 values for 5-LO. Thus, we speculated that SOG might also suppress RANKL-induced osteoclastogenesis through inhibition of 5-LO activity and blockage of production of 5-LO catalytic products, leukotrienes. 5-LO expression silence by targeted siRNA confirmed that the suppressive effects of 5-LO inhibition on osteoclastogenesis, implicated that SOG attenuated RANKL-mediated osteoclastogenesis via inhibiting 5-LO activity. The stronger inhibitory effect of SOG on osteoclast formation at late stage might be attributed to blocking autocrine of leukotrienes. Meanwhile, our results further demonstrated that NFATc1 expression was downregulated by silence of 5-LO, but phosphorylation of AKT and GSK3β was not markedly affected. These results suggested that the suppressive effects of SOG was independent of its inhibition on 5-LO activity. The inhibitory effects of SOG on RANKL-induced osteoclastogenesis might arise from the inhibition of both of 5-LO activity and AKT- GSK3β signaling.

Further, we established LPS-induced bone loss model to investigate whether SOG existed therapeutic effects on inflammatory bone loss in vivo. We found that SOG effectively rescued LPS-induced bone loss as demonstrated by H&E staining and Micro-CT of femurs. The number of osteoclasts was decreased by SOG treatment by TRAP staining, which is consistent with the result in vitro.

In conclusion, SOG attenuated formation and function of osteoclast through suppressing AKT-mediated GSK3β inactivation, and 5-LO catalytic activity. But, SOG did not affect NF-κB, MAPK and AKT-GSK3β signaling in response to RANKL transient stimulation. Moreover, SOG prevented LPS-induced bone loss in mice through inhibiting osteoclastogenesis.

Declarations

Ethics declarations

Animal experiments were performed strictly according to the Guide for the Humane Use and Care of Laboratory Animals (Animal protocol number: TJCAC-018-036).

Consent for publication

Not applicable

Availability of data and materials

The datasets used and/or analysed during the current study are available from the corresponding author on reasonable request.

Competing interests

The authors declare that they have no competing interests.

Founding

This study was supported by National Natural Science Foundation (Grant no. 31670347, 81001369 and 31170327).

Authors' contributions

HBW, CZ, WCS designed research; JJC and MXZ performed research; CMW contributed new reagents or ananlytic tools; XYC, MLS and QSP analyzed data; JJC wrote the paper.

Ackonwledgements

We acknowledge and appreciate our colleagues for their valuable efforts and comments on this paper.

Authors' information

Affiliations

Putuo People's Hospital, School of Life Sciences and Technology, Tongji University, Shanghai 200092, China

Jinjin Cao, Xinyan Chen, Menglu Sun, Congmin Wei, Zhou Cheng and Hongbing Wang

Department of Neurology, Ruikang Hospital of Guangxi TCM University, Nanning 530011, China

Mingxue Zhou

Key Laboratory of Zoonoses Research, Ministry of Education, Institute of Zoonosis, Jilin University, Changchun 130062, PR China

Qisheng Peng and Wanchun Sun

References

1. Min SK, Kang HK, Jung SY, Jang DH, Min BM. A vitronectin-derived peptide reverses ovariectomy-induced bone loss via regulation of osteoblast and osteoclast differentiation. Cell Death Differ. 2018;25(2):268–81.
2. Taubman MA, Valverde P, Han X, Kawai T. Immune response: the key to bone resorption in periodontal disease. Journal of periodontology. 2005;76(11 Suppl):2033–41.
3. Liu YC, Lerner UH, Teng YT. Cytokine responses against periodontal infection: protective and destructive roles. Periodontology 2000. 2010;52(1):163–206.
4. Yuan K, Mei J, Shao D, et al. Cerium Oxide Nanoparticles Regulate Osteoclast Differentiation Bidirectionally by Modulating the Cellular Production of Reactive Oxygen Species. International journal of nanomedicine. 2020;15:6355–72.
5. Takayanagi H. Osteoimmunology: shared mechanisms and crosstalk between the immune and bone systems. Nat Rev Immunol. 2007;7(4):292–304.
6. Boyce BF, Xing L. Functions of RANKL/RANK/OPG in bone modeling and remodeling. Archives of biochemistry biophysics. 2008;473(2):139–46.
7. Boyle WJ, Simonet WS, Lacey DL. Osteoclast differentiation and activation. Nature. 2003;423(6937):337–42.
8. Boyce BF. Advances in the regulation of osteoclasts and osteoclast functions. J Dent Res. 2013;92(10):860–7.
9. Negishi-Koga T, Takayanagi H. Ca2+-NFATc1 signaling is an essential axis of osteoclast differentiation. Immunological reviews. 2009;231(1):241–56.
10. Moon JB, Kim JH, Kim K, et al. Akt induces osteoclast differentiation through regulating the GSK3β/NFATc1 signaling cascade. J Immunol. 2012;188(1):163–9.
11. Grimes CA, Jope RS. CREB DNA binding activity is inhibited by glycogen synthase kinase-3 beta and facilitated by lithium. Journal of neurochemistry. 2001;78(6):1219–32.
12. Shin J, Jang H, Lin J, Lee SY. PKCbeta positively regulates RANKL-induced osteoclastogenesis by inactivating GSK-3beta. Mol Cells. 2014;37(10):747–52.
13. Hu L, Sun J, Li H, et al. Differential mechanistic investigation of protective effects from imperatorin and sec-O-glucosylhamaudol against arsenic trioxide-induced cytotoxicity in vitro. Toxicology in vitro: an international journal published in association with BIBRA. 2016;37:97–105.
14. Koh GH, Song H, Kim SH, et al. Effect of sec-O-glucosylhamaudol on mechanical allodynia in a rat model of postoperative pain. The Korean journal of pain. 2019;32(2):87–96.
15. Liu G, Xie J, Shi Y, et al. Sec-O-glucosylhamaudol suppressed inflammatory reaction induced by LPS in RAW264.7 cells through inhibition of NF-κB and MAPKs signaling. *Bioscience reports.* 2020;40(2).
16. Zhao A, Li L, Li B, Zheng M, Tsao R. Ultrafiltration. LC-ESI-MSn screening of 5-lipoxygenase inhibitors from selected Chinese medicinal herbs Saposhnikovia divaricata, Smilax glabra, Pueraria lobata and Carthamus tinctorius. Journal of Functional Foods. 2016;24:244–53.

17. Xiao L, Zhong M, Huang Y, et al. Puerarin alleviates osteoporosis in the ovariectomy-induced mice by suppressing osteoclastogenesis via inhibition of TRAF6/ROS-dependent MAPK/NF-κB signaling pathways. 2020;12(21):21706–21729.
18. Boyce BF, Xiu Y, Li J, Xing L, Yao Z. NF-kappaB-Mediated Regulation of Osteoclastogenesis. Endocrinol Metab (Seoul). 2015;30(1):35–44.
19. Lee K, Chung YH, Ahn H, Kim H, Rho J, Jeong D. Selective Regulation of MAPK Signaling Mediates RANKL-dependent Osteoclast Differentiation. Int J Biol Sci. 2016;12(2):235–45.
20. Kim JH, Kim N. Regulation of NFATc1 in Osteoclast Differentiation. J Bone Metab. 2014;21(4):233–41.
21. Neal JW, Clipstone NA. Glycogen synthase kinase-3 inhibits the DNA binding activity of NFATc. The Journal of biological chemistry. 2001;276(5):3666–73.
22. Asagiri M, Sato K, Usami T, et al. Autoamplification of NFATc1 expression determines its essential role in bone homeostasis. J Exp Med. 2005;202(9):1261–9.
23. Matsushita T, Chan YY, Kawanami A, Balmes G, Landreth GE, Murakami S. Extracellular signal-regulated kinase 1 (ERK1) and ERK2 play essential roles in osteoblast differentiation and in supporting osteoclastogenesis. Molecular cellular biology. 2009;29(21):5843–57.
24. Mukherjee K, Chattopadhyay N. Pharmacological inhibition of cathepsin K: A promising novel approach for postmenopausal osteoporosis therapy. Biochemical Pharmacology. 2016;117:10–9.
25. Miyamoto T. Regulators of osteoclast differentiation and cell-cell fusion. The Keio journal of medicine. 2011;60(4):101–5.
26. Chiu YH, Ritchlin CT. DC-STAMP: A Key Regulator in Osteoclast Differentiation. J Cell Physiol. 2016;231(11):2402–7.
27. Amirhosseini M, Madsen RV, Escott KJ, Bostrom MP, Ross FP, Fahlgren A. GSK-3beta inhibition suppresses instability-induced osteolysis by a dual action on osteoblast and osteoclast differentiation. J Cell Physiol. 2018;233(3):2398–408.
28. Wei J, Li Y, Liu Q, et al. Betulinic Acid Protects From Bone Loss in Ovariectomized Mice and Suppresses RANKL-Associated Osteoclastogenesis by Inhibiting the MAPK and NFATc1 Pathways. Front Pharmacol. 2020;11:1025.
29. Golden LH, Insogna KL. The expanding role of PI3-kinase in bone. Bone. 2004;34(1):3–12.
30. Lee SE, Woo KM, Kim SY, et al. The phosphatidylinositol 3-Kinase, p38, and extracellular signal-regulated kinase pathways are involved in osteoclast differentiation. Bone. 2002;30(1):71–7.
31. Xiao D, Zhou Q, Gao Y, et al. PDK1 is important lipid kinase for RANKL-induced osteoclast formation and function via the regulation of the Akt-GSK3β-NFATc1 signaling cascade. Journal of cellular biochemistry. 2020;121(11):4542–57.
32. Jang HD, Shin JH, Park DR, et al. Inactivation of glycogen synthase kinase-3beta is required for osteoclast differentiation. The Journal of biological chemistry. 2011;286(45):39043–50.

33. Yan D-Y, Tang J, Chen L, et al. Imperatorin promotes osteogenesis and suppresses osteoclast by activating AKT/GSK3 β/β-catenin pathways. 2020;24(3):2330–2341.
34. Bouchareychas L, Grossinger EM, Kang M, Qiu H, Adamopoulos IE. Critical Role of LTB4/BLT1 in IL-23-Induced Synovial Inflammation and Osteoclastogenesis via NF-kappaB. J Immunol. 2017;198(1):452–60.
35. Chen ZK, Lv HS, Jiang J. LTB4 can stimulate human osteoclast differentiation dependent of RANKL. Artif Cells Blood Substit Immobil Biotechnol. 2010;38(1):52–6.
36. Hikiji H, Ishii S, Yokomizo T, Takato T, Shimizu T. A distinctive role of the leukotriene B4 receptor BLT1 in osteoclastic activity during bone loss. Proceedings of the National Academy of Sciences of the United States of America. 2009;106(50):21294–9.
37. Lee JM, Park H, Noh AL, et al. 5-Lipoxygenase mediates RANKL-induced osteoclast formation via the cysteinyl leukotriene receptor 1. J Immunol. 2012;189(11):5284–92.
38. Paula-Silva FWG, Arnez MFM, Petean IBF, et al. Effects of 5-lipoxygenase gene disruption on inflammation, osteoclastogenesis and bone resorption in polymicrobial apical periodontitis. Arch Oral Biol. 2020;112:104670.
39. Kang JH, Ting Z, Moon MR, et al. 5-Lipoxygenase inhibitors suppress RANKL-induced osteoclast formation via NFATc1 expression. Bioorg Med Chem. 2015;23(21):7069–78.
40. Cao J, Wang S, Wei C, et al. Agrimophol suppresses RANKL-mediated osteoclastogenesis through Blimp1-Bcl6 axis and prevents inflammatory bone loss in mice. Int Immunopharmacol. 2021;90:107137.
41. Moussa FM, Cook BP, Sondag GR, et al. The role of miR-150 regulates bone cell differentiation and function. *Bone.* 2020:115470.
42. Chen Y, Lu J, Li S, et al. Carnosol attenuates RANKL-induced osteoclastogenesis in vitro and LPS-induced bone loss. Int Immunopharmacol. 2020;89(Pt A):106978.
43. Seo W, Lee S, Tran PT, et al. 3-Hydroxyolean-12-en-27-oic Acids Inhibit RANKL-Induced Osteoclastogenesis in Vitro and Inflammation-Induced Bone Loss in Vivo. *Int J Mol Sci.* 2020;21(15).

Figures

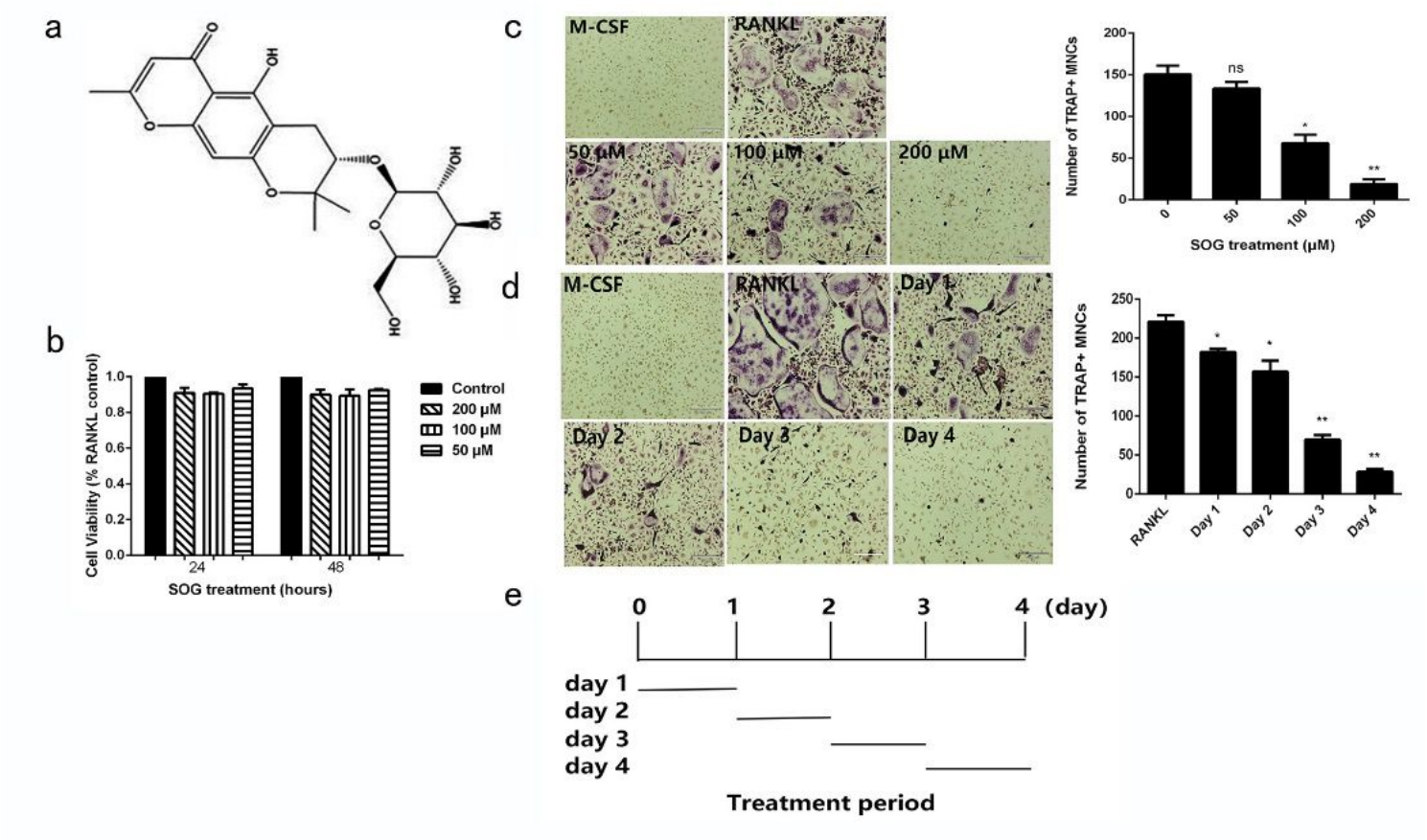

Figure 1

SOG inhibits RANKL-induced osteoclastogenesis. (a) Chemical structure of Sec-O-glucosylhamaudol (SOG) (b) BMMs were seeded on 96-well plates and cultured for 24 h and 48 h in α-MEM complete medium containing 30 ng/mL M-CSF, 100 ng/mL RANKL and indicated concentrations of SOG (0-200 μM). Cell viability was determined by MTT assay. (c) BMMs were seeded in 48-well-plates and cultured in α-MEM complete medium containing 30 ng/mL M-CSF, 100 ng/mL RANKL and different concentrations of SOG for 4 d and subsequently for TRAP staining (left panel). TRAP activity (at 100× magnification, left panel) and the number of TRAP+ osteoclasts with ≥ 3 nuclei (right panel). Scale bar = 190 μm (d) Effects of 200 μM SOG on RANKL-induced osteoclast differentiation from BMMs at different stage of cell differentiation. TRAP activity (at 100× magnification, left panel) and the number of TRAP+ osteoclasts with ≥3 nuclei (right panel). Scale bar = 190 μm. (e) Treatment time of SOG for figure 1d. All experiments were performed at least three times, *$p < 0.05$ and **$p < 0.01$ versus RANKL induced group.

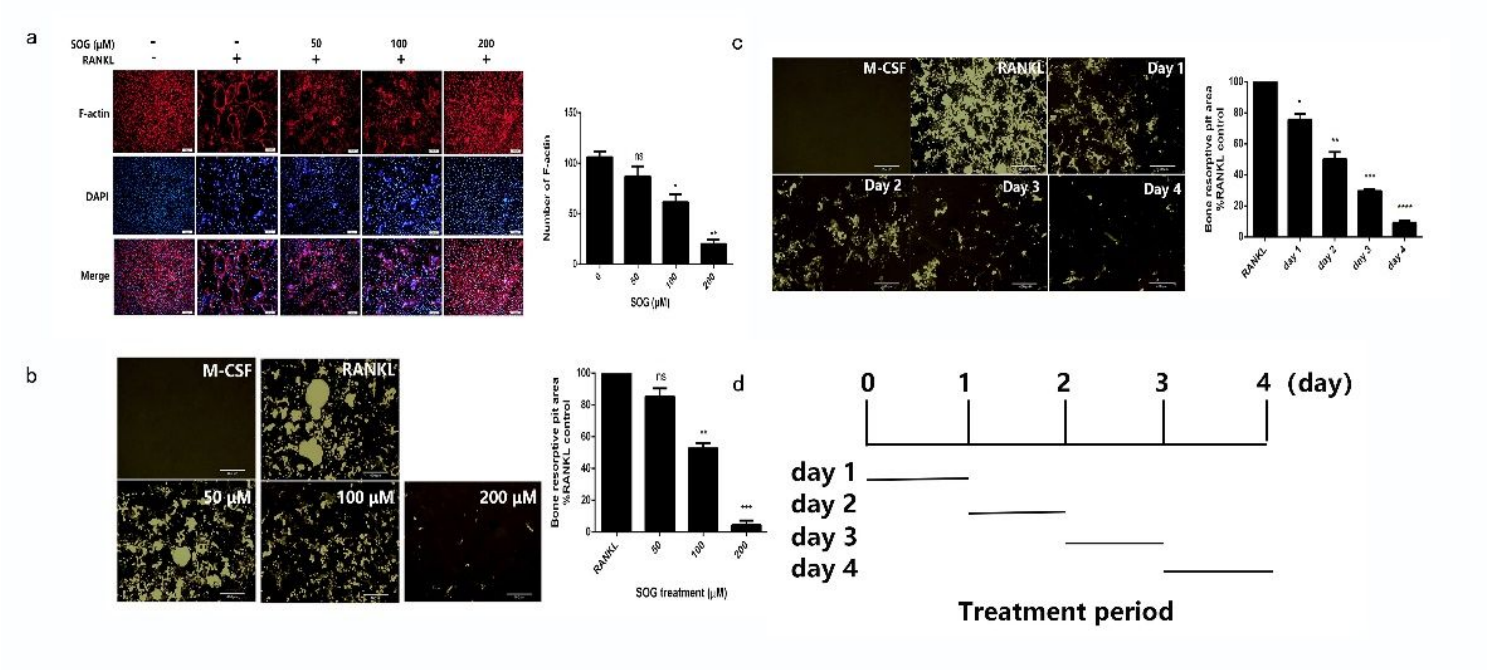

Figure 2

SOG repressed F-actin ring formation and bone resorption. (a) BMMs were seeded in 48-well-plates and cultured in α-MEM complete medium containing 30 ng/mL M-CSF, 100 ng/mL RANKL and different concentrations of SOG for 4 d. Cells were then fixed with 4% PFA and stained for F-actin ring and observed via fluorescence microscope (left panel). 100× magnification. Scale bars, 100 μm. Quantification of F-actin rings (right panel). (b) BMMs were cultured on a corning osteo assay surface multiple well plate with α-MEM complete medium containing 30 ng/mL M-CSF, 100 ng/mL RANKL and different concentrations of SOG for 4 days. At the end of culture, cells were removed and modified Vonkonsa staining was performed. The resorption pit areas were observed at a light microscope. 40× magnification. Scale bars, 460 μm. Quantification of resorption area per view area (right panel). (c) Indicated concentrations of SOG were added to medium at indicated time point during cell culture period. At the end of culture, cells were removed and modified Vonkonsa staining was performed. The resorption pit areas were observed at a light microscope. 40× magnification. Scale bars, 460 μm. Quantification of resorption pit areas per view area (right panel). (d) Treatment time of SOG for figure 2c. All experiments were performed at least three times, *p < 0.05, **p < 0.01, ***p < 0.001 and ****p < 0.0001 versus RANKL induced group.

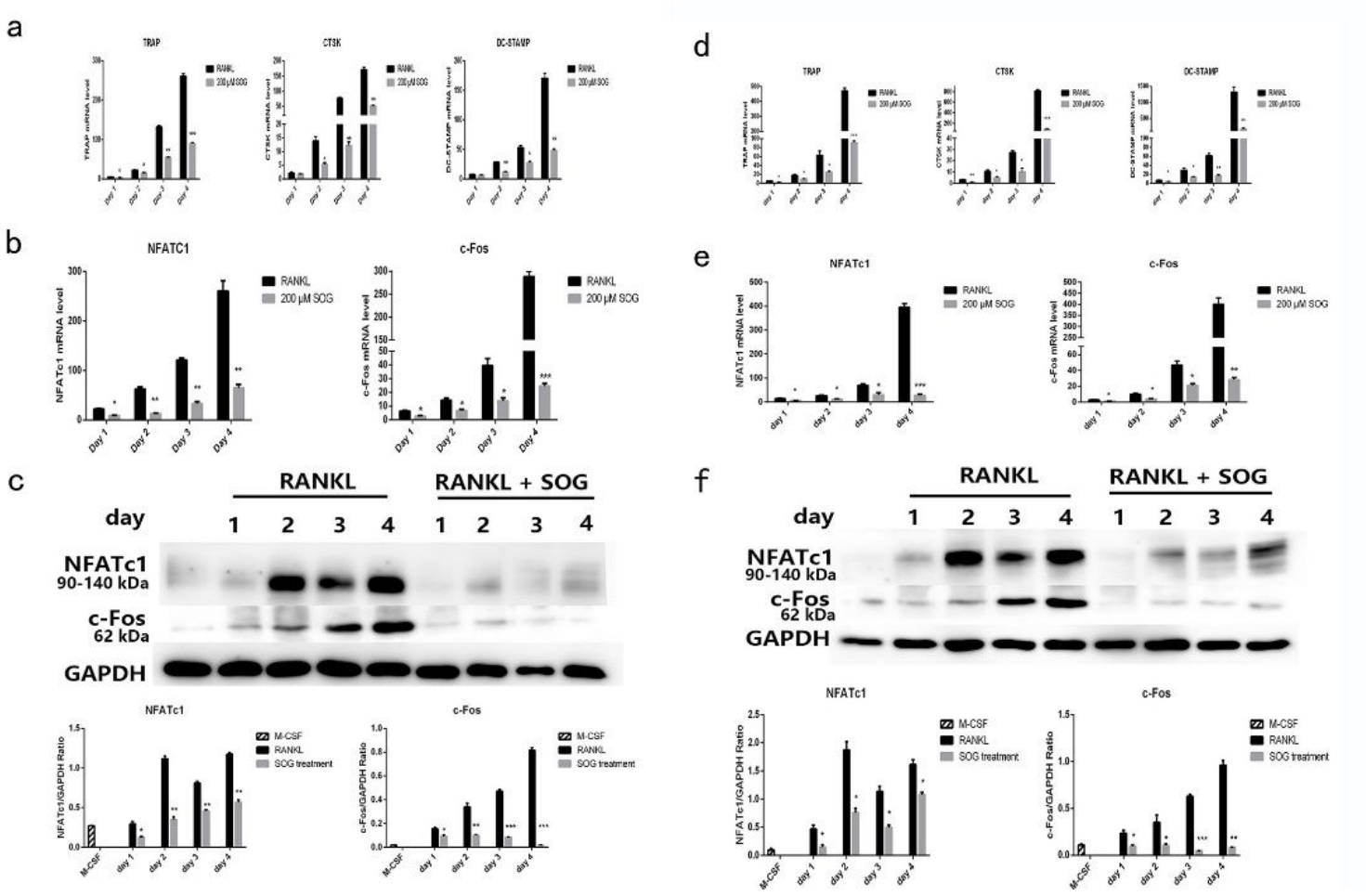

Figure 3

SOG reduced RANKL-induced expression of c-Fos, NFATc1 and osteoclast-specific genes. BMMs were cultured in α-MEM completed medium containing 30 ng/mL M-CSF, 100 ng/mL RANKL and 200 μM SOG for 4 days. (a) The mRNA levels of TRAP, CTSK and DC-STAMP were determined by realtime-PCR analysis. (b) The mRNA levels of c-Fos and NFATc1 were determined by realtime-PCR analysis. (c) The protein levels of c-Fos and NFATc1 were determined by western blotting analysis (upper panel). Relative protein expression was calculated using Image J (down panel). BMMs were cultured in α-MEM completed medium containing 30 ng/mL M-CSF, 100 ng/mL RANKL and 200 μM SOG at different periods of osteoclastogenesis. (d) The mRNA levels of TRAP, CTSK and DC-STAMP were analyzed by realtime-PCR. (e) The mRNA levels of c-Fos and NFATc1 were determined by realtime-PCR ananlysis. (f) Protein levels of c-Fos and NFATc1 (upper panel) were examined using western blotting assay. Relative protein expression was calculated using Image J (down panel). All experiments were performed at least three times, *$p < 0.05$, **$p < 0.01$, and ***$p < 0.001$ versus RANKL induced group.

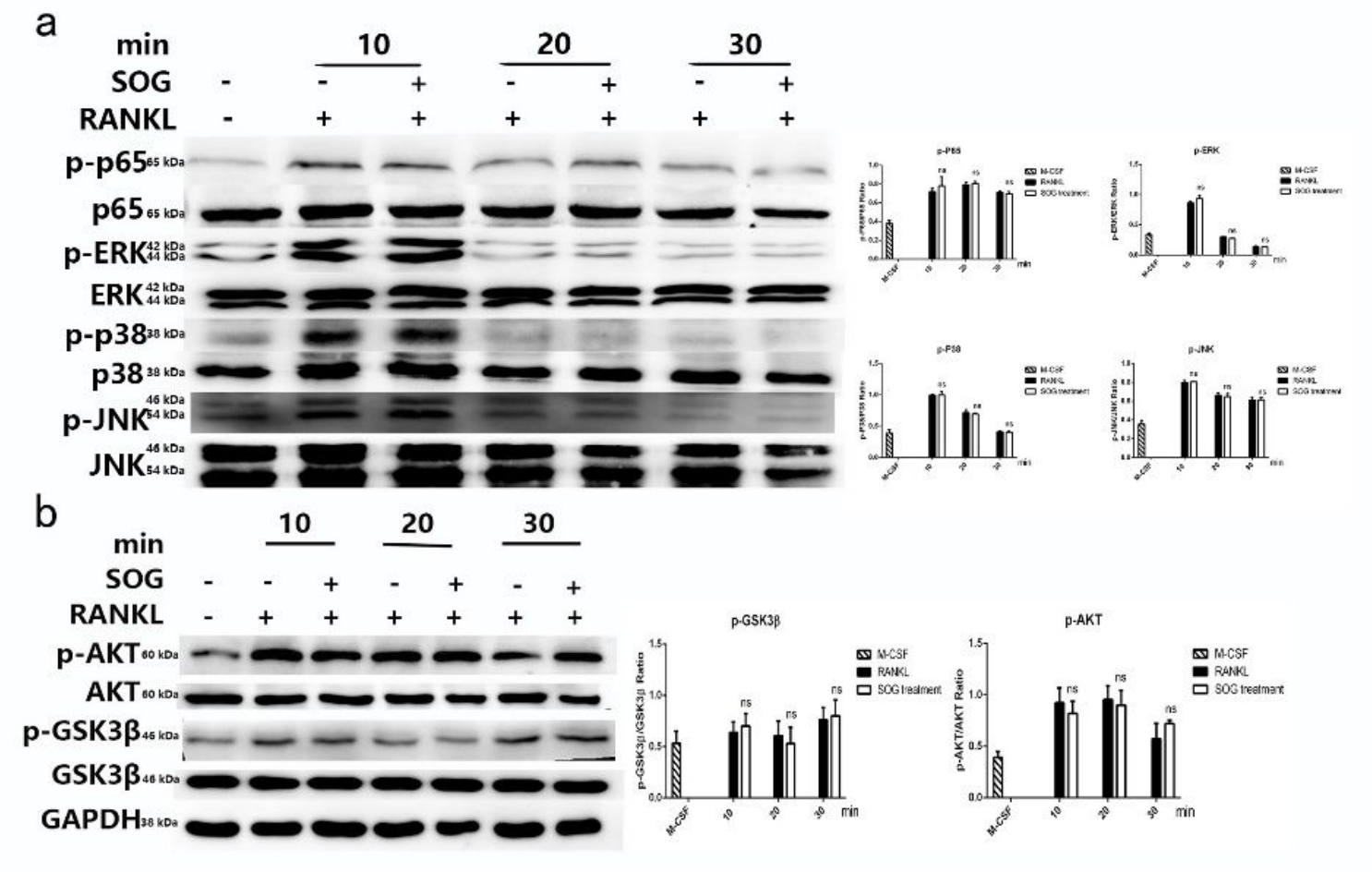

Figure 4

The effects of SOG on RANKL-induced NF-κB, MAPK, AKT-GSK3β signaling pathway. BMMs were pretreated with or without 200 μM SOG for 4 h. Then the cells were stimulated with 80 ng/mL RANKL for 0, 10, 20, 30 min. Cell lysates were analyzed using Western blotting with specific antibodies. (a) NF-κB and MAPK signaling pathway (left panel). Relative protein expression was calculated using ImageJ (right panel). (b) AKT-GSK3β signaling pathway (left panel). Relative protein expression was calculated using ImageJ (right panel). The relative band intensity of phosphorylated proteins was normalized to that of the un-phosphorylated protein and represented as a graph. All experiments were performed at least three times, ns: not significant.

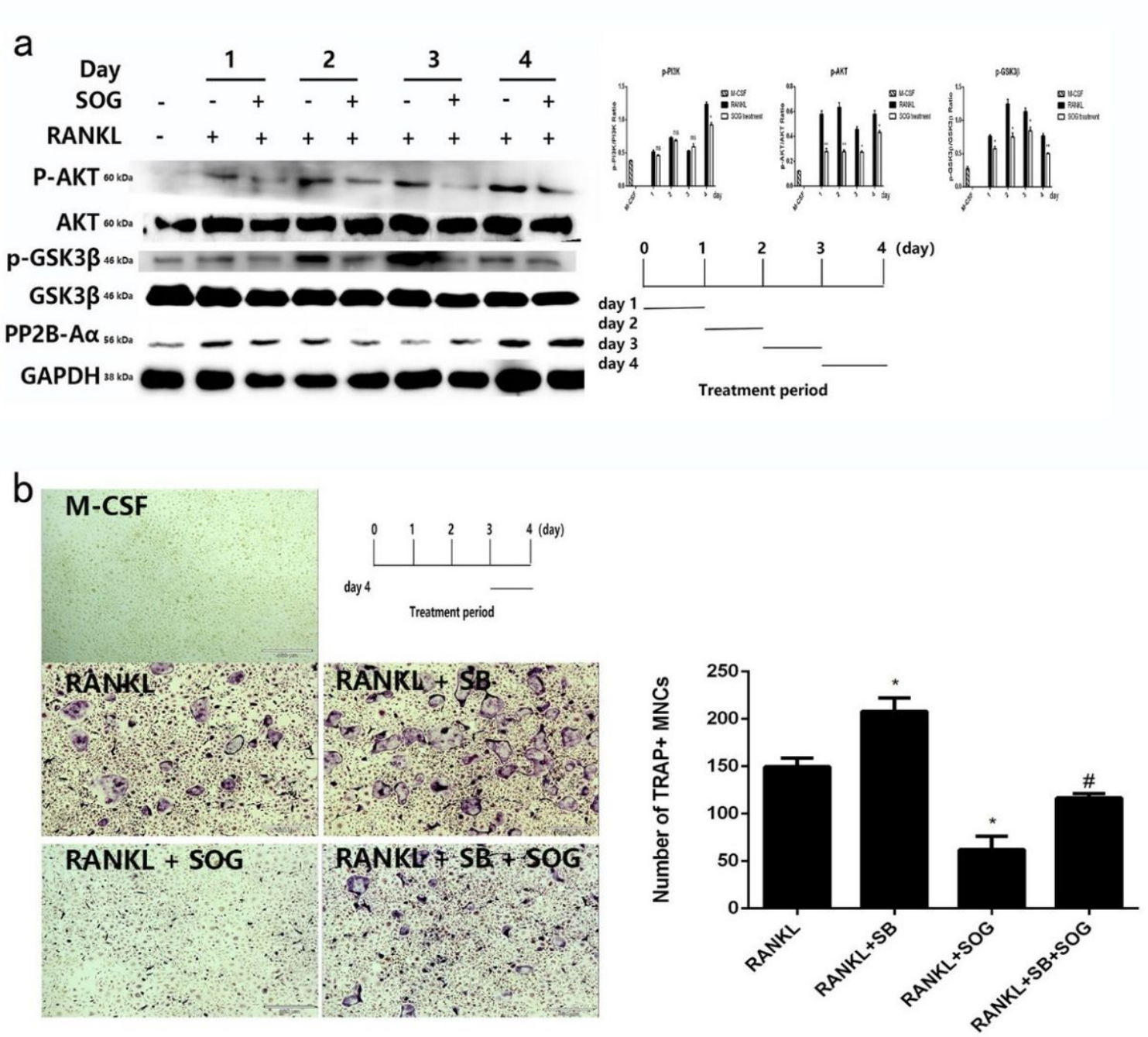

Figure 5

The effect of SOG on RANKL-induced calcineurin and AKT-GSK3β signaling pathway. (a) BMMs were cultured in α-MEM completed medium containing 30 ng/mL M-CSF, 100 ng/mL RANKL and 200 μM SOG at different periods of osteoclastogenesis. The protein levels of calcimeurin, AKT and GSK3β were analyzed using Western blotting with specific antibodies (left panel). Relative protein expression was calculated using Image J and treatment time of SOG (lower right panel). (b) BMMs were cultured in α-MEM complete medium containing 30 ng/mL M-CSF, 100 ng/mL RANKL and 200 μM SOG or 10 μM SB415286 (SB) at day 3 of osteoclastogenesis. at the end culture, cells were stained by TRAP staining (left panel) and treatment time of SOG (upper left panel). The TRAP+ cells with ≥ 3 nuclei were counted (right panel). 40× magnification. Scale bars, 460 μm. All experiments were performed at least three times,

ns: not significant, *p < 0.05, **p < 0.01 and ***p < 0.001 versus RANKL induced group. #p < 0.05 versus RANKL + SB induced group.

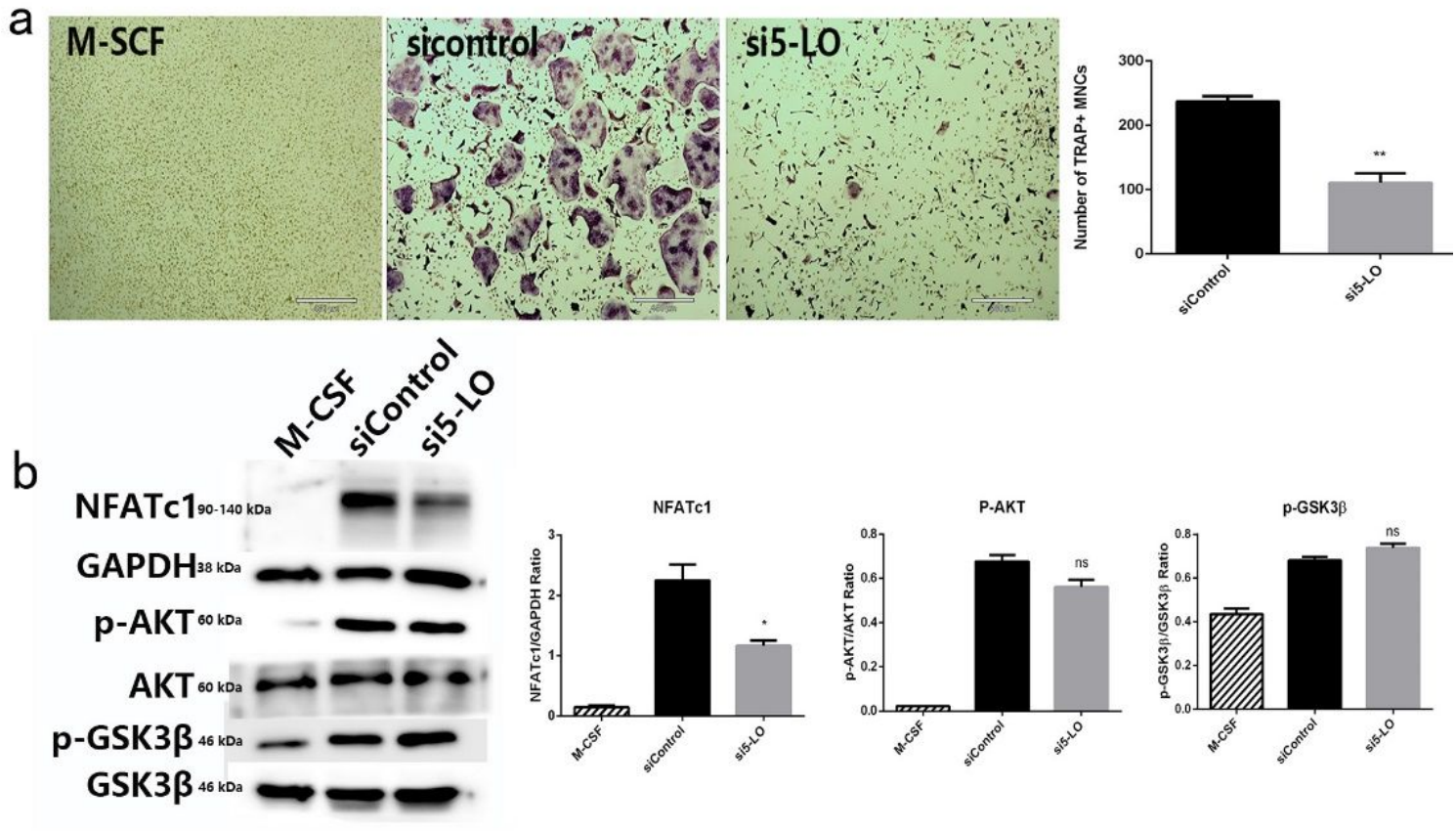

Figure 6

The effects of Knockdown of 5-LO on RANKL-induced osteoclastogenesis. BMMs were plated and cultured on 48 wells or 6 wells plates at 37 ℃ for 24 h. Next, BMMs were transfected with control siRNA or 5-LO targeted siRNA at a final concentration of 50 nM for indicated time.(a) cells were stained using TRAP staining (left panel). The number of TRAP+ osteoclasts with ≥3 nuclei (right panel). 40× magnification. Scale bars, 460 μm. (b) Protein expression levels of NFATc1, AKT and GSK3β were analyzed using Western blotting with specific antibodies (left panel). Relative protein expression was calculated using Image J (right panel). All experiments were performed at least three times, ns: not significant, *p < 0.05 and **p < 0.01 versus sicontrol group.

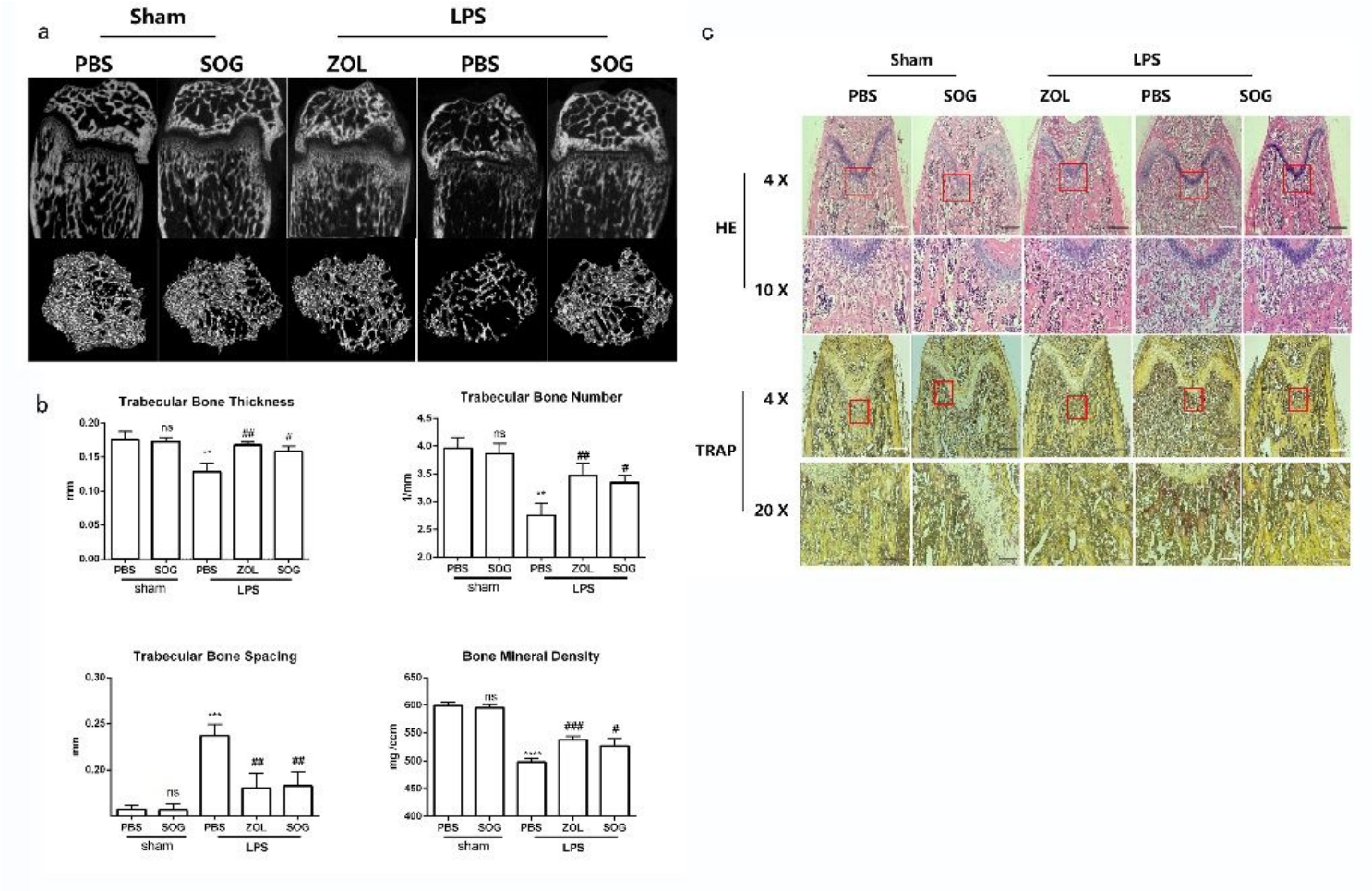

Figure 7

SOG improved LPS-induced bone loss in mice. (a) Representative 2D and 3D reconstructions of Micro-CT scan of femurs. (b) Bone mineral density (BMD), trabecular number (Tb. N), trabecular separation (Tb. Sp) and trabecular thickness (Tb. Th) of femurs were quantified by analyzing Micro-CT data using the CT analyzer software. (c) Representative histological sections of femoral bone tissue sections were stained with H&E (at 40× and 100× magnification) and TRAP staining (at 40× and 200× magnification) and Data are expressed as means ± SD. ns: no significance, *p < 0.05, **p < 0.01, and ***p < 0.001 relative to respective sham group; #p < 0.05, ##p < 0.01, and ###p < 0.001 relative to LPS group.